Perovskites

How to cite:
International Edition: doi.org/10.1002/anie.202208875
German Edition: doi.org/10.1002/ange.202208875

Hybrid Germanium Bromide Perovskites with Tunable Second Harmonic Generation

Yang Liu, Ya-Ping Gong, Shining Geng, Mei-Ling Feng, Despoina Manidaki, Zeyu Deng, Constantinos C. Stoumpos, Pieremanuele Canepa, Zewen Xiao, Wei-Xiong Zhang, and Lingling Mao**

Abstract: Ge-based hybrid perovskite materials have demonstrated great potential for second harmonic generation (SHG) due to the geometry and lone-pair induced non-centrosymmetric structures. Here, we report a new family of hybrid 3D Ge-based bromide perovskites $A\mathrm{GeBr_3}$, $A = \mathrm{CH_3NH_3}$ (MA), $\mathrm{CH(NH_2)_2}$ (FA), Cs and $\mathrm{FAGe_{0.5}Sn_{0.5}Br_3}$, crystallizing in polar space groups. These compounds exhibit tunable SHG responses, where $\mathrm{MAGeBr_3}$ shows the strongest SHG intensity (5 × potassium dihydrogen phosphate, KDP). Structural and theoretical analysis indicate the high SHG efficiency is attributed to the displacement of Ge^{2+} along [111] direction and the relatively strong interactions between lone pair electrons of Ge^{2+} and polar MA cations along the *c*-axis. This work provides new structural insights for designing and fine-tuning the SHG properties in hybrid metal halide materials.

Introduction

Hybrid metal halide perovskites have been recognized as high-performance photovoltaic materials and reached remarkable power conversion efficiency over the past decade.[1–5] Other areas of optoelectronic applications, such as, light-emitting diodes (LEDs),[6–10] lasing[11–14] and photodetectors have also been extensively explored.[15–19] It is important to explore other areas of optoelectronics for these high performance semiconductors to realize their full potential.[20–23]

The abundant structural diversity and favorable physical properties[24–26] prompt hybrid metal halide perovskites as attractive candidates in the field of nonlinear optical (NLO) applications. Second harmonic generation (SHG) as one of the most fundamental NLO processes, exhibits strict symmetry dependence for nonlinear polarization of materials, requiring non-centrosymmetric structures.[27,28] An important task in the field of NLO applications is to explore the correlation between the structure of hybrid metal halide perovskites and their NLO properties, which would facilitate further optimization for NLO applications, including all-optical modulation,[29,30] multiphoton microscopy,[31,32] high-resolution optical lithography,[33] optical limiting[34–37] and THz generation/detection.[38,39] Common metal halide perovskites usually crystallize in centrosymmetric space groups, especially the three-dimensional parent perovskites structures.[26] It still remains a challenge to design perovskite-based materials that break inversion symmetry in search for strong SHG responses.[40]

A effective strategy to obtain SHG-active materials is through the introduction of chiral or asymmetric organic components.[41–44] Yuan et al. fabricated non-centrosymmetric perovskite materials with efficient SHG signal by utilizing chiral ammonium cations.[44] Pb-based chloride perovskites by employing 1-methylhydrazinium cation

[*] Dr. Y. Liu, Prof. Dr. L. Mao
Department of Chemistry, SUSTech Energy Institute for Carbon Neutrality, Southern University of Science and Technology
Shenzhen, Guangdong 518055 (P. R. China)
E-mail: maoll@sustech.edu.cn

Y.-P. Gong, Prof. Dr. W.-X. Zhang
MOE Key Laboratory of Bioinorganic and Synthetic Chemistry, School of Chemistry, Sun Yat-Sen University
Guangzhou, Guangdong 510275, (P. R. China)

S. Geng, Prof. Dr. Z. Xiao
Wuhan National Laboratory for Optoelectronics, Huazhong University of Science and Technology
Wuhan, Hubei 430074, (P. R. China)

Prof. Dr. M.-L. Feng
State Key Laboratory of Structural Chemistry, Fujian Institute of Research on the Structure of Matter, Chinese Academy of Sciences
Fuzhou, Fujian 350002 (P. R. China)

D. Manidaki, Prof. Dr. C. C. Stoumpos
Department of Materials Science and Technology, University of Crete
Heraklion, 70013 (Greece)

Dr. Z. Deng, Prof. Dr. P. Canepa
Department of Materials Science and Engineering, National University of Singapore
Singapore, 117575 (Singapore)
E-mail: pcanepa@nus.edu.sg

Prof. Dr. P. Canepa
Department of Chemical and Biomolecular Engineering, National University of Singapore
Singapore, 117585 (Singapore)

$(CH_3NH_2NH_2^+)$ has been reported to have an unusual temperature-activated, reversible SHG response.[43] A four-state switchable SHG behavior from $(Me_3NNH_2)_2[CdI_4]$ was reported, correlating with molecular dynamics of the polar organic cations.[45]

Another perhaps more effective strategy for obtaining non-centrosymmetric structure for metal halide perovskites is to utilize stereochemically active lone pair metal cations (Ge^{2+}, Sn^{2+} etc.) and the interplay between ionic radius and the tolerance factor.[46–51] Chen et al. reported a series of hybrid metal halide $(C_6H_5(CH_2)_4NH_3)_4MX_7{\cdot}H_2O$ (M = Bi, In, X = Br or I) with SHG responses.[46] Previously, we have reported a series of Ge-based iodide perovskites with excellent SHG properties.[48] The SHG intensity can also be tuned by Br/Cl solid solutions in $CsGe(Br_xCl_{1-x})_3$.[52] $CsGeBr_3$ was recently reported to be ferroelectric with clear SHG responses.[51] In the bromide-based system, as the ionic radius decreases from Pb to Ge, the tolerance factor has largely increased for $AGeBr_3$ (A = Cs, MA and FA), compared with the Pb- and Sn-based analogues (Figure 1). Despite the large tolerance factors, which are 0.95, 1.09 and 1.18 for the $AGeBr_3$ (A = Cs, MA and FA) series, fall outside of the region of 0.8–1 for a stable perovskite structure.[53] The Ge–Br perovskites have shown strong off-centering and crystallize in the non-centrosymmetric space group $R3m$, which enables them to be strong SHG materials.

Here, based on the prototype compound $CsGeBr_3$, we synthesize four new hybrid Ge-based bromide perovskites ($MAGeBr_3$, $FAGeBr_3$ and $FA_{0.5}MA_{0.5}GeBr_3$, $FAGe_{0.56}Sn_{0.44}Br_3$, MA = CH_3NH_3, FA = $CH(NH_2)_2$) (Figure 2), crystallizing in polar space groups at room temperature. With changing the A-site cation and M-site metal alloying, the distortion of $[MBr_6]$ octahedra change remarkably, following the trend with band gap increasing in the order of $CsGeBr_3 < FAGe_{0.56}Sn_{0.44}Br_3 < MAGeBr_3 < FA_{0.5}MA_{0.5}GeBr_3 < FAGeBr_3$. Among the compounds, only $CsGeBr_3$ exhibits photoluminescence (PL) emission at room temperature. SHG measurements reveal that $CsGeBr_3$, $MAGeBr_3$ and $FA_{0.5}MA_{0.5}GeBr_3$ display a strong SHG response, with $MAGeBr_3$ exhibiting the strongest response. We interpret these results as a direct consequence of the structural distortion of the octahedra, which lead to a polar arrangement of lone pair electrons on Ge^{2+}. According to structural analysis and theoretical calculations, the stronger

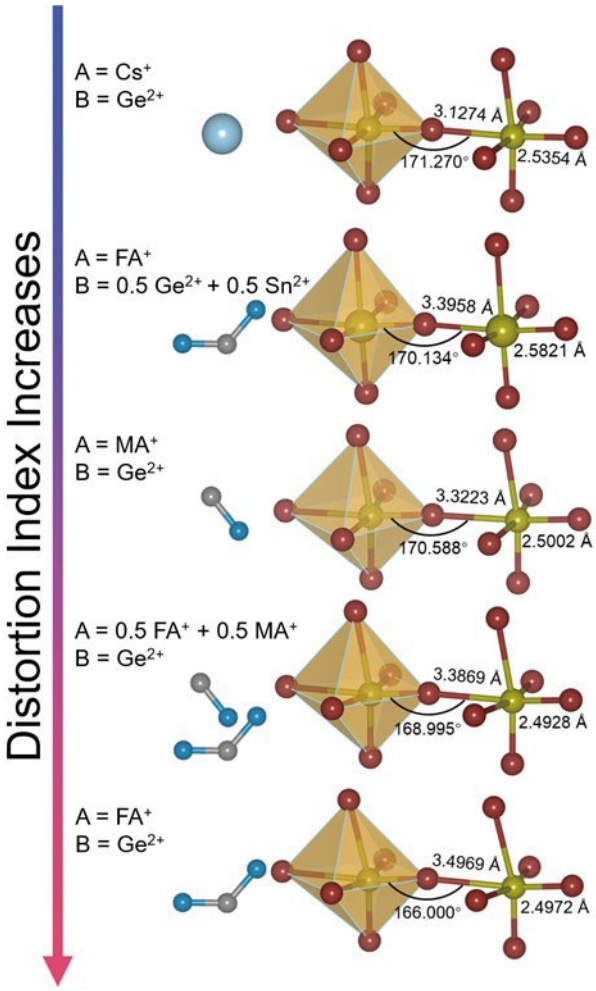

Figure 2. Distortion index trend and bond length of all compounds with different organic cations or mixed metal cations at room temperature. Color code: Cs, cyan; Ge/Sn, lime; Br, red; C, grey; N, blue. Hydrogen atoms are omitted for clarity.

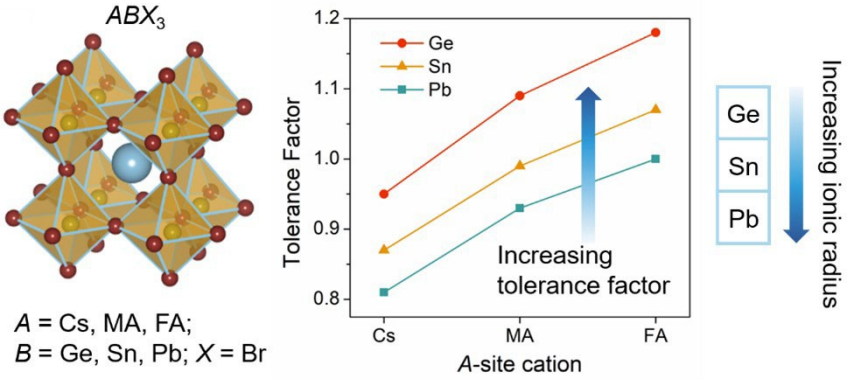

Figure 1. The generic structure and tolerance factors for different ABX_3 (A = Cs, MA and FA; B = Ge, Sn, Pb; X = Br) combinations.

distortion on the Ge^{2+} octahedra is induced by the polar MA cations ($C3v$ point group), which further polarizes the octahedra along the body diagonal of the perovskite cages. This work highlights the importance of using lone-pair active metals and choosing the appropriate organic cations to enhance SHG in hybrid metal halide materials.

Results and Discussion

The synthetic procedure for the new Ge-based bromide perovskites reported here is similar to previously reported Ge-based metal halides.[48,52,54] ABr (A = Cs or MA) or FA(AcO) and GeO_2 are dissolved in concentrated aqueous HBr and H_3PO_2 (reducing agent), under heating and stirring at ≈126 °C (boiling point of the azeotrope). Crystalline solids are obtained by slow cooling at room temperature without perturbation (see Supporting Information). $CsGeBr_3$, $MAGeBr_3$, $FAGeBr_3$ and $FA_{0.5}MA_{0.5}GeBr_3$ all crystallize in the non-centrosymmetric trigonal space group $R3m$ at room temperature, and they are isomorphic with the reported AGeI$_3$ (A = Cs, MA and FA).[48] The anionic [$GeBr_3$] units are triangular pyramids, with the lone pair electrons of Ge^{2+} along the proper threefold rotation axis running parallel to the crystallographic c-axis (Figures S8a and S11). The active lone pair is located between the triplet of bromide ions that have longer bonding distances, opposite to the triplet of short, covalent Ge–Br bonds. The active lone pairs along with one another pointing towards the same direction contribute to the overall uncompensated dipole moment of the Ge^{2+} octahedra along the crystallographic c-axis.[24,25,48,49,52,54] The [$GeBr_6$] octahedra are connected three-dimensionally in a corner-sharing fashion with the A-site cation sitting in the middle void. For the arrangement of the cations in AGeBr$_3$ (A = Cs, MA and FA), both Cs and MA ($C3v$ symmetry) are located on the c-axis (Figure S11). However, for FA, only one C–N bond of it is aligned along the c-axis and the other triple-disordered C–N bond exhibits a $C3v$ symmetry around the c-axis (Figure S8a). The distortion of the [$GeBr_6$] octahedra increases with the increasing organic cation size (Figure 2 and Table 1), which is accompanied by the change of bond length and angle, as well as the displacement of Ge^{2+} along the [111] direction in the unit cell (Tables S6–S9 and Figure S6).[51,55] Noted that there are two kinds of Ge–Br bonds (short and long bond) due to the prominent lone pair effect of Ge^{2+}. In all compounds, the short bonds remain virtually constant, and range from 2.49–2.54 Å for the AGeBr$_3$ family. While the long bonds increase as the organic cation size increases, ranging from 3.13–3.50 Å. The Ge–Br–Ge angles also decrease as the degree of distortion increases, ranging from 166.0–171.3° (Table S7). Moreover, these changes in bond length and angle are more dramatic than that of AGeI$_3$ (Table S8).[48] We further synthesize the solid solution of Ge and Sn based on the most distorted compound $FAGeBr_3$. With an experimental molar ratio of 1:1 (Ge: Sn), the obtained metal alloyed compound $FAGe_{0.5}Sn_{0.5}Br_3$ was characterized by single-crystal X-ray diffraction and the formula was refined to be $FAGe_{0.56}Sn_{0.44}Br_3$. Unlike the parent Ge^{2+} compound $FAGe_{0.56}Sn_{0.44}Br_3$ crystallizes in the orthorhombic space group $Cmc2_1$ at room temperature, without changing the salient features of the structure. Following the incorporation of Sn and due to lowering of the symmetry, two Ge/Sn–Br short bonds at 2.5821(25) and one short bond at 2.5909(34) Å are present, with the lone pair located on the opposite side between the three longer bonds with bond lengths of 3.3958(29) (two bonds) and 3.3915(37) Å (one bond). The corresponding Ge/Sn–Br–Ge/Sn bond angles are in the range of 170.1–175.6° (Tables S6 and S7). Compared with $FAGeBr_3$, the incorporation of Sn brings the bond length and angle closer to $CsGeBr_3$, and the distortion of the [Ge/SnBr$_6$] octahedra decreases accordingly. As depicted in Figures 2, S6 and Table 1, the distortion index of $FAGe_{0.56}Sn_{0.44}Br_3$ is between $CsGeBr_3$ and $MAGeBr_3$.

To investigate whether the compounds undergo the typical perovskite phase transitions, low-temperature single crystal data were collected. The single-crystal data of $MAGeBr_3$ $FA_{0.5}MA_{0.5}GeBr_3$, and $FAGe_{0.5}Sn_{0.5}Br_3$ have not been obtained due to poor diffraction quality at low-temperature. For $CsGeBr_3$, the unit cell volume shrinks with decreasing temperature, and no space group change was observed. However, $FAGeBr_3$ shows clear phase transition behavior, and its space group changes to Cm at low temperatures. For $FAGeBr_3$, the arrangement of anionic [$GeBr_3$] units in the lattice changes, one Ge–Br band is parallel to the c-axis and the other two Ge–Br bonds are the mirror image of each other (mirror plane: [010] plane) and locate on [001] plane. Meanwhile, the FA cation becomes ordered and lays parallel to [010] plane (Figure S8b). Thermogravimetric analysis suggests that all compounds are stable up to approximately 500 K under nitrogen atmosphere (Figures 3 and S4). Such phase transition behavior in this system should arise from the disorder/order of the

Table 1: Space group, bond length distortion (D) and bond angle variance (σ^2) for all compounds.

Compound	Temperature [K]	Space group	D [Å]	σ^2 [°]
$CsGeBr_3$	298	$R3m$	0.10455	21.3167
$CsGeBr_3$	100	$R3m$	0.09452	18.2440
$MAGeBr_3$	298	$R3m$	0.14120	24.6935
$FAGeBr_3$	298	$R3m$	0.16677	77.2124
$FAGeBr_3$	100	Cm	0.15392	73.9935
$FA_{0.5}MA_{0.5}GeBr_3$	298	$R3m$	0.15206	36.9292
$FAGe_{0.5}Sn_{0.5}Br_3$	298	$Cmc2_1$	0.13536	29.6146

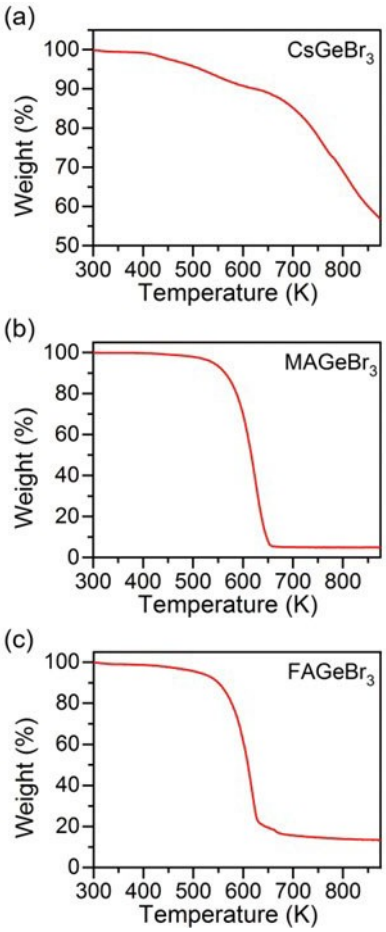

Figure 3. Thermogravimetric analysis (TGA) for $CsGeBr_3$ (a), $MAGeBr_3$ (b) and $FAGeBr_3$ (c).

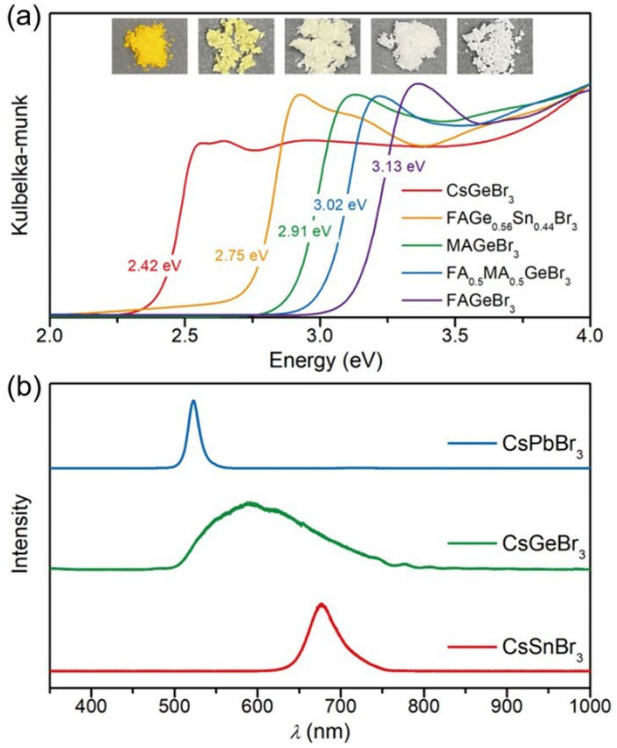

Figure 4. a) Optical absorption spectra of all compounds. Top: pictures of all crystalline compounds (the order of arrangement: $CsGeBr_3$, $FAGe_{0.56}Sn_{0.44}Br_3$, $MAGeBr_3$, $FA_{0.5}MA_{0.5}GeBr_3$, $FAGeBr_3$); b) Normalized PL emission spectrum (excited at 325 nm) at room temperature for $CsGeBr_3$, $CsSnBr_3$ and $CsPbBr_3$.

organic cations at high/low temperature according to structural analysis. In addition, it should be mentioned that the phase transition behavior will likely to change the structural polarity (*R*3*m* (polar)→*Cm* (polar) for $FAGeBr_3$). The temperature-dependent phase transitions enable these hybrid compounds to possibly become stimuli-responsive switchable SHG materials.[43,45,56–64]

The optical absorption spectra of these Ge-based bromide perovskite materials are shown in Figure 4a, where the band gaps ranging from 2.42 eV ($CsGeBr_3$), 2.91 eV ($MAGeBr_3$) to 3.13 eV ($FAGeBr_3$). It is consistent with the gradual color change of these compouds (yellow→pale yellow→colorless) (see Figure 4a top). The measured optical band gaps appear in good agreement with the fundamental gaps predicted for $CsGeBr_3$ (2.25 eV), $MAGeBr_3$ (2.98 eV) and $FAGeBr_3$ (3.43 eV) by hybrid functional DFT calculations (Figure S6 and Table S13). These materials all show sharp absorption edges, with no clear excitonic features.[48] For $CsGeBr_3$, $MAGeBr_3$ and $FAGeBr_3$, the increasing trend of the band gap are similar to previously reported iodide analogues.[48] The band gap evolution is also consistent with the bond length distortion (*D*) (Table 1), where larger distortion clearly leads to a larger band gap.

Due to the mixed cations FA and MA, it seems quite reasonable that the band gap of $FA_{0.5}MA_{0.5}GeBr_3$ is between $MAGeBr_3$ and $FAGeBr_3$. Then, we evaluate the relationship between the band gap and the structure below. As depicted in Figure S6, for $AGeBr_3$ (A = Cs, MA and FA), it shows clear rules that the increasing band gap is positively correlated with long bond length and is accompanied by the decreasing Ge–Br–Ge angle. Thus, we attribute such an increasing tendency of the band gap to the decrease of orbital overlap of [$GeBr_6$] units, and the larger the organic cation size, the less the orbital overlap in this system. $FAGe_{0.56}Sn_{0.44}Br_3$ should be treated differently in the analysis of the band gap. Due to the band gap energy of Sn-based 3D halide perovskites are generally lower than that of Ge-based 3D halide perovskites,[65,66] thus it's understandable that band gap energy of $FAGe_{0.56}Sn_{0.44}Br_3$ is the lowest in the organic-inorganic hybrid system reported here.

Steady-state PL measurements were performed at room temperature under a He-Cd laser excitation (325 nm). As shown in Figure 4b, only $CsGeBr_3$ exhibits a broad emission band around 588 nm (2.11 eV), which is directly related to the minimum band gap energy of $CsGeBr_3$ in this system. Meanwhile, Lü et al. reveal a general relationship that the best PL performance can be obtained by tuning the degree of off-centering distortion towards 0.2 in halide perovskites.[67] Therefore, it is taken for granted that only CsGeBr3, which has the smallest $D_{\text{off-center}}$ value here

(Table S9) exhibits PL performance. Compared with the narrow PL spectra of $CsPbBr_3$ (523 nm)[68] and $CsSnBr_3$ (676 nm),[65] $CsGeBr_3$ has a large full width at half maximum (FWHM) of 144 nm, compared with $CsPbBr_3$ (18 nm), $CsSnBr_3$ (47 nm) and covers a wider emission range, such wide PL peak is common in Ge-based halides.[69–71] The origin of the broad emission may be attributed to the presence of self-trapped excitons caused by transient structural defect states according to the reported literature.[72,73]

Because of the non-centrosymmetric nature of these compounds, polycrystalline powder SHG measurements under 1064 nm laser irradiation were performed at room temperature, with potassium dihydrogen phosphate (KDP) used as the reference. It shows that $CsGeBr_3$, $MAGeBr_3$ and $FA_{0.5}MA_{0.5}GeBr_3$ are highly SHG active (Figure 5a), with $MAGeBr_3$ having the strongest SHG signal. To the best of our knowledge, among many SHG-active crystalline 3D halide perovskites (Table S10), the SHG intensity of $MAGeBr_3$ has the best SHG property with 5.3 times that of KDP compared with some lead-based perovskites (e.g. the SHG intensity of $MhyPbBr_3$ is 0.18 times than that of KDP[74]). However, the SHG intensity of these compounds

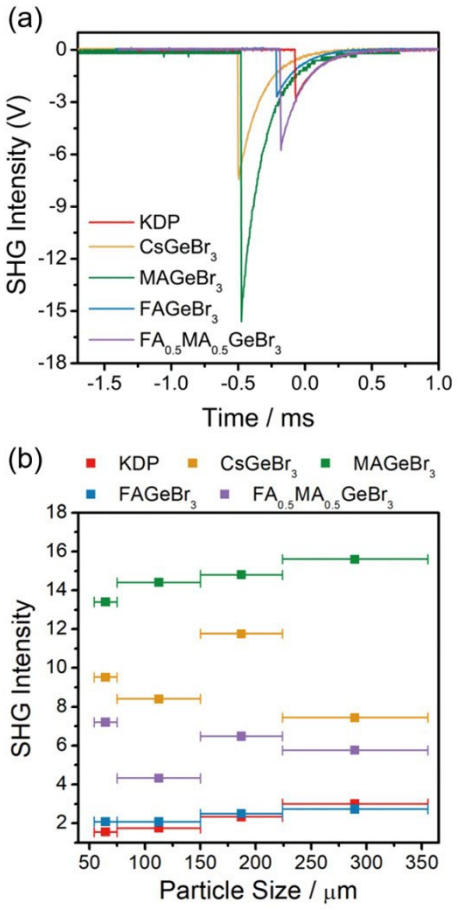

Figure 5. a) SHG intensity of $CsGeBr_3$, $MAGeBr_3$, $FAGeBr_3$, $FA_{0.5}MA_{0.5}GeBr_3$ and KDP under particle size range (224–355 μm) at room temperature. b) SHG intensity of $CsGeBr_3$, $MAGeBr_3$, $FAGeBr_3$, $FA_{0.5}MA_{0.5}GeBr_3$ and KDP with different particle sizes at room temperature.

does not decrease with increasing band gap as previously reported,[75,76] which may be related to the orientation of the *A*-site cation. This will be discussed in greater detail in the subsequent theoretical calculations section. In addition, the particle size dependent measurements show that the SHG intensity of $MAGeBr_3$ increases with increasing particle size[77] (phase-matchable) and the SHG intensity of $CsGeBr_3$ and $FA_{0.5}MA_{0.5}GeBr_3$ fluctuates with increasing particle size (non-phase-matchable). $FAGeBr_3$ shows the lowest SHG response here, but alloying it with MA significantly increases the SHG intensity (Figure 5). It is worth mentioning that $FAGe_{0.56}Sn_{0.44}Br_3$ is easily oxidized and sensitive to humidity, so we are unable to obtain reliable SHG results. Although there are many studies on the size-dependent SHG of $CsGeBr_3$,[52,55] our results show a similar trend with our previously reported $AGeI_3$ (A = Cs, MA, FA).[48] We further calculate the computed $\chi^{(2)}$ from the structures. The $\chi^{(2)}$ (0.28 pm V^{-1}) for KDP obtained in our hybrid density functional theory (DFT) calculations appear in reasonable agreement with the measured value (0.38 pm V^{-1}).[78] The overall trend within the series is very similar to the iodide analogues.[48] In line with previous experimental data, DFT predicts the $\chi^{(2)}_{xyy}$ ($CsGeI_3$) > $\chi^{(2)}_{xyy}$ ($CsGeBr_3$) as shown in Table S14. Furthermore, as suggested by the diffraction experiments, the initial computed model of $MAGeBr_3$ for $\chi^{(2)}$ assumed the C of the MA cation pointing towards the Br- (I-) species. Notwithstanding the complexity in describing the positional disorder of $FAGeBr_3$, the computed $\chi^{(2)}$ values are lower than both $MAGeBr_3$ and $CsGeBr_3$, and in line with the experimental trend of Figure 5.

$CsGeBr_3$, $MAGeBr_3$ and $FAGeBr_3$ were chosen as representative compounds to discuss the relationship between *A*-site cations with respect to the electronic structure. As shown in Figure 6, all calculated compounds have direct (fundamental) band gaps, and calculated to be 2.24 eV for $CsGeBr_3$ 2.98 eV for $MAGeBr_3$ and 3.43 eV for $FAGeBr_3$, respectively. The predicted band gaps are in good agreement with the experimental observations. For all the compounds, both valence band maximum (VBM) and conduction band minimum (CBM) are located at the A point, where the VBM consists of the non-bonding states of Ge 4p orbitals and CBM consists of the antibonding states of Ge 4s and Br 4p orbitals. It appears that the *A*-site cations still affect the density of states distribution of Ge 4s, Ge 4p and Br 4p orbitals by affecting the distortion of crystal structures. As a result, the relative position of the CBM is shifted to higher energies by replacing the larger *A*-site cation.[79] $FAGeBr_3$ exhibits slightly flatter band dispersion compared with $CsGeBr_3$ and $MAGeBr_3$, which is indicative of poorer charge carrier mobilities. To elucidate this aspect, we have computed the average electron (m_e) and hole effective (m_h) masses along the high symmetry directions, which are listed in Table S15. These values suggest that all calculated compounds have good semiconducting properties along the high symmetry directions.

ELF analysis for these three compounds is also conducted to visualize the interatomic interactions. As shown in Figures 7, S8a and S11, it displays strong interatomic interactions along the shorter Ge–Br bonds, and compara-

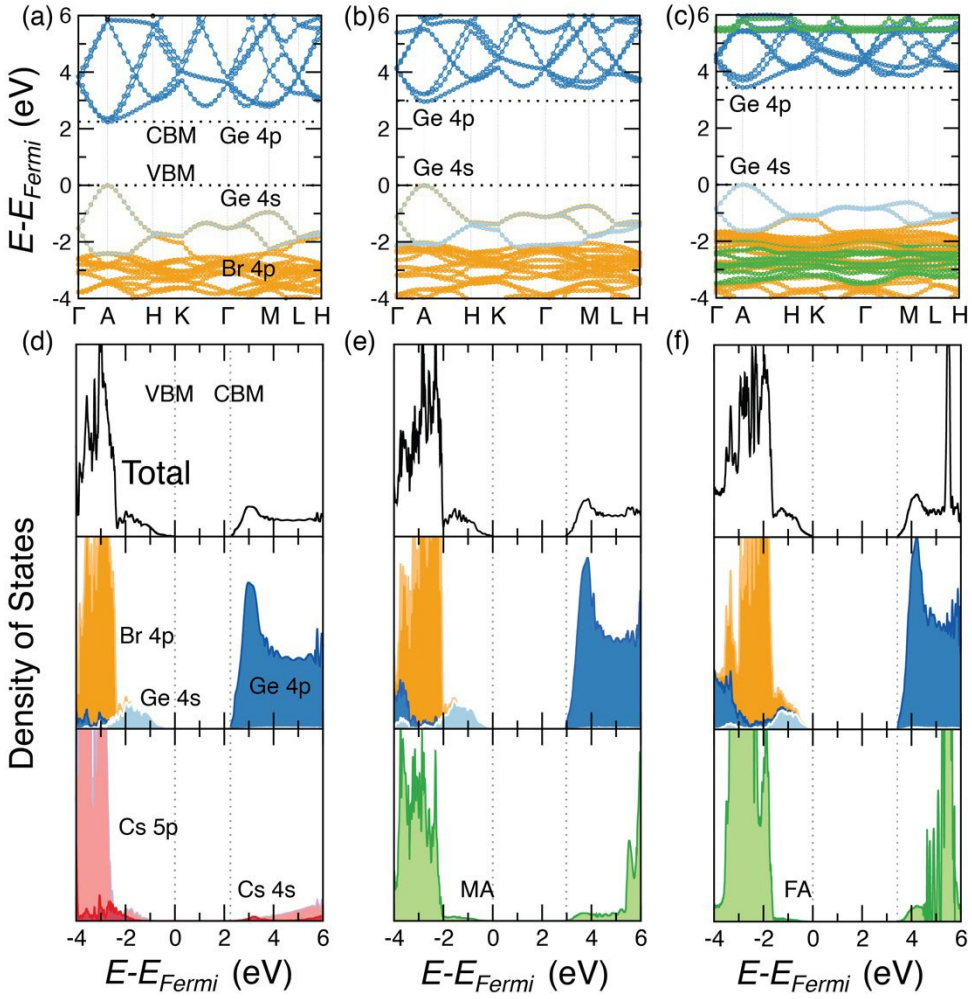

Figure 6. Calculated band structures of $CsGeBr_3$ (a), $MAGeBr_3$ (b) and $FAGeBr_3$ (c); Calculated projected densities of states of $CsGeBr_3$ (d), $MAGeBr_3$ (e) and $FAGeBr_3$ (f). VMB and CBM indicate the valence band maxima and conduction band minima giving, and their difference is the fundamental band gap. Both band structures and density of states were obtained from hybrid functional density functional calculations (PBE0-D3).

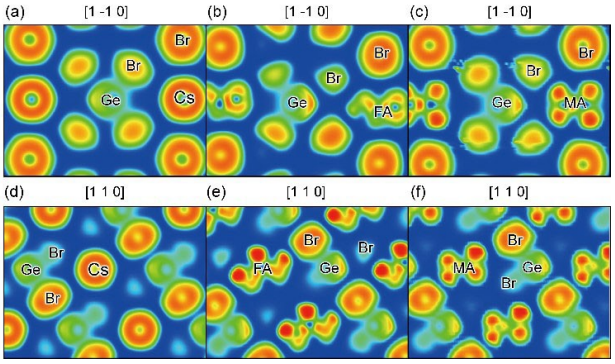

Figure 7. Sliced-plane of electron localization functions (ELF) diagrams for $CsGeBr_3$ (a), $MAGeBr_3$ (b) and $FAGeBr_3$ (c) along the [1−10] plane, and $CsGeBr_3$ (d), $MAGeBr_3$ (e) and $FAGeBr_3$ (f) along the [110] plane. The labels of the atoms are provided in the diagrams.

tively weaker interatomic interactions along the longer Ge–Br bonds. At the same time, it is also observed that the $4s^2$ lone pair is located on the opposite side of the short Ge–Br bonds, and has non-negligible interactions with *A*-site cations. In comparison, the interactions between MA cations and $4s^2$ lone pair is the strongest, which stems from the polar nature of the MA and results in the largest SHG response reported here (see Figure S11).[80,81] Such strong interactions can also be more intuitively reflected in the structural analysis, it is obvious that the distance between Ge^{2+} and MA is the shortest (5.2218 Å for $CsGeBr_3$, 4.6305 Å for $MAGeBr_3$ and 5.0590 Å for $FAGeBr_3$). Additionally, the SHG response is directly related to the polarity of the crystal, which can be evaluated by the local dipole moment of each polar group (organic cation and $[GeBr_6]$ unit) and its geometric arrangement.[82,83] As we know, the dipole moment for MA (about 2.3 D) is higher than FA (about 0.2 D) and Cs (non-polar),[84,85] which could potentially explain the overall better performance of $MAGeBr_3$.

Conclusion

We have successfully synthesized and characterized a series of SHG-active hybrid bromide perovskite materials utilizing Ge^{2+} for its sterically active lone pair and strong off-centering originating from the smaller ionic radius compared with Sn^{2+} and Pb^{2+}. The introduction of hybrid organic cations (MA and FA), metal cations (Ge and Sn) and alloying both at *A*- and *B*-site, respectively, highly diversify the structure, optical, electronic and non-linear optical properties of these materials. Among the four new compounds reported here, $MAGeBr_3$ exhibits the largest SHG response due to the proper orientation of the polar cation MA along with the direction of the lone pair (twice as large than that of $CsGeBr_3$). Moreover, these hybrid organic-inorganic compounds have potential temperature-dependent phase transition behaviors, demonstrating that these compounds could serve as excellent candidates for next generation switchable SHG materials. Our work showcases the importance of structural tunability from hybrid organic cations in combination with the proper choice of metal cation in developing efficient hybrid NLO materials.

Acknowledgements

This work was supported by SUSTech start-up grant (Y01216150). The authors are grateful to the assistance of SUSTech Core Research Facilities. P. C. acknowledges support from the Singapore Ministry of Education Academic Fund Tier 1 (R-284-000-186-133). The computational work for this article was partially performed on resources of the National Supercomputing Centre, Singapore (https://www.nscc.sg).

Conflict of Interest

The authors declare no competing financial interest.

Data Availability Statement

The data that support the findings of this study are available from the corresponding author upon reasonable request.

Keywords: Halide Perovskites · Non-Centrosymmetric Structure · Non-Linear Optics · Second Harmonic Generation

[1] I. Chung, B. Lee, J. He, R. P. H. Chang, M. G. Kanatzidis, *Nature* **2012**, *485*, 486–489.
[2] M. M. Lee, J. Teuscher, T. Miyasaka, T. N. Murakami, H. J. Snaith, *Science* **2012**, *338*, 643–647.
[3] H.-S. Kim, C.-R. Lee, J.-H. Im, K.-B. Lee, T. Moehl, A. Marchioro, S.-J. Moon, R. Humphry-Baker, J.-H. Yum, J. E. Moser, M. Grätzel, N.-G. Park, *Sci. Rep.* **2012**, *2*, 591.
[4] J. Jeong, M. Kim, J. Seo, H. Lu, P. Ahlawat, A. Mishra, Y. Yang, M. A. Hope, F. T. Eickemeyer, M. Kim, Y. J. Yoon, I. W. Choi, B. P. Darwich, S. J. Choi, Y. Jo, J. H. Lee, B. Walker, S. M. Zakeeruddin, L. Emsley, U. Rothlisberger, A. Hagfeldt, D. S. Kim, M. Grätzel, J. Y. Kim, *Nature* **2021**, *592*, 381–385.
[5] A. Kojima, K. Teshima, Y. Shirai, T. Miyasaka, *J. Am. Chem. Soc.* **2009**, *131*, 6050–6051.
[6] X.-K. Liu, W. Xu, S. Bai, Y. Jin, J. Wang, R. H. Friend, F. Gao, *Nat. Mater.* **2021**, *20*, 10–21.
[7] J.-S. Yao, J.-J. Wang, J.-N. Yang, H.-B. Yao, *Acc. Chem. Res.* **2021**, *54*, 441–451.
[8] L. N. Quan, F. P. García de Arquer, R. P. Sabatini, E. H. Sargent, *Adv. Mater.* **2018**, *30*, 1801996.
[9] S. D. Stranks, H. J. Snaith, *Nat. Nanotechnol.* **2015**, *10*, 391–402.
[10] Y.-H. Kim, J. S. Kim, T.-W. Lee, *Adv. Mater.* **2019**, *31*, 1804595.
[11] Q. Zhang, Q. Shang, R. Su, T. T. H. Do, Q. Xiong, *Nano Lett.* **2021**, *21*, 1903–1914.
[12] L. Lei, Q. Dong, K. Gundogdu, F. So, *Adv. Funct. Mater.* **2021**, *31*, 2010144.
[13] C. Qin, A. S. D. Sandanayaka, C. Zhao, T. Matsushima, D. Zhang, T. Fujihara, C. Adachi, *Nature* **2020**, *585*, 53–57.
[14] J. Qin, X.-K. Liu, C. Yin, F. Gao, *Trends Chem.* **2021**, *3*, 34–46.
[15] F. P. García de Arquer, A. Armin, P. Meredith, E. H. Sargent, *Nat. Rev. Mater.* **2017**, *2*, 16100.
[16] M. Ahmadi, T. Wu, B. Hu, *Adv. Mater.* **2017**, *29*, 1605242.
[17] H. Gu, S.-C. Chen, Q. Zheng, *Adv. Opt. Mater.* **2021**, *9*, 2001637.
[18] Y. Zhang, Y. Ma, Y. Wang, X. Zhang, C. Zuo, L. Shen, L. Ding, *Adv. Mater.* **2021**, *33*, 2006691.
[19] H.-P. Wang, S. Li, X. Liu, Z. Shi, X. Fang, J.-H. He, *Adv. Mater.* **2021**, *33*, 2003309.
[20] M. Kepenekian, J. Even, *J. Phys. Chem. Lett.* **2017**, *8*, 3362–3370.
[21] J. Wang, C. Zhang, H. Liu, R. McLaughlin, Y. Zhai, S. R. Vardeny, X. Liu, S. McGill, D. Semenov, H. Guo, R. Tsuchikawa, V. V. Deshpande, D. Sun, Z. V. Vardeny, *Nat. Commun.* **2019**, *10*, 129.
[22] X.-F. Cheng, W.-H. Qian, J. Wang, C. Yu, J.-H. He, H. Li, Q.-F. Xu, D.-Y. Chen, N.-J. Li, J.-M. Lu, *Small* **2019**, *15*, 1905731.
[23] L. Zhou, Y.-F. Xu, B.-X. Chen, D.-B. Kuang, C.-Y. Su, *Small* **2018**, *14*, 1703762.
[24] A. Ferrando, J. P. Martínez Pastor, I. Suárez, *J. Phys. Chem. Lett.* **2018**, *9*, 5612–5623.
[25] Y. Zhou, Y. Huang, X. Xu, Z. Fan, J. B. Khurgin, Q. Xiong, *Appl. Phys. Rev.* **2020**, *7*, 041313.
[26] J. Xu, X. Li, J. Xiong, C. Yuan, S. Semin, T. Rasing, X.-H. Bu, *Adv. Mater.* **2020**, *32*, 1806736.
[27] Y. R. Shen, *The Principles of Nonlinear Optics*, Wiley, New York, **1984**.
[28] R. A. Ganeev, *Nonlinear Optical Refraction and Absorption of Media*, Springer, Dordrecht, **2013**.
[29] G. Grinblat, I. Abdelwahab, M. P. Nielsen, P. Dichtl, K. Leng, R. F. Oulton, K. P. Loh, S. A. Maier, *ACS Nano* **2019**, *13*, 9504–9510.
[30] L. Wu, K. Chen, W. Huang, Z. Lin, J. Zhao, X. Jiang, Y. Ge, F. Zhang, Q. Xiao, Z. Guo, Y. Xiang, J. Li, Q. Bao, H. Zhang, *Adv. Opt. Mater.* **2018**, *6*, 1800400.
[31] Y. Fan, Y. Wang, N. Zhang, W. Sun, Y. Gao, C.-W. Qiu, Q. Song, S. Xiao, *Nat. Commun.* **2019**, *10*, 2085.
[32] J. Yu, Z. Li, Y. Liao, C. Kolodziej, S. Kuyuldar, W. S. Warren, C. Burda, M. C. Fischer, *Adv. Opt. Mater.* **2019**, *7*, 1901185.
[33] N. Zhang, W. Sun, S. P. Rodrigues, K. Wang, Z. Gu, S. Wang, W. Cai, S. Xiao, Q. Song, *Adv. Mater.* **2017**, *29*, 1606205.
[34] T.-C. Wei, S. Mokkapati, T.-Y. Li, C.-H. Lin, G.-R. Lin, C. Jagadish, J.-H. He, *Adv. Funct. Mater.* **2018**, *28*, 1707175.
[35] S. J. Varma, J. Cherusseri, J. Li, J. Kumar, E. Barrios, J. Thomas, *AIP Adv.* **2020**, *10*, 045130.

[36] K. S. Rao, R. A. Ganeev, K. Zhang, Y. Fu, G. S. Boltaev, S. K. Maurya, C. Guo, *Opt. Mater.* **2019**, *92*, 366–372.
[37] S. Zou, G. Yang, T. Yang, D. Zhao, Z. Gan, W. Chen, H. Zhong, X. Wen, B. Jia, B. Zou, *J. Phys. Chem. Lett.* **2018**, *9*, 4878–4885.
[38] A. Chanana, Y. Zhai, S. Baniya, C. Zhang, Z. V. Vardeny, A. Nahata, *Nat. Commun.* **2017**, *8*, 1328.
[39] K. Cong, E. Vetter, L. Yan, Y. Li, Q. Zhang, Y. Xiong, H. Qu, R. D. Schaller, A. Hoffmann, A. F. Kemper, Y. Yao, J. Wang, W. You, H. Wen, W. Zhang, D. Sun, *Nat. Commun.* **2021**, *12*, 5744.
[40] T. W. Kasel, Z. Deng, A. M. Mroz, C. H. Hendon, K. T. Butler, P. Canepa, *Chem. Sci.* **2019**, *10*, 8187–8194.
[41] H. Jo, X. Chen, H.-S. Lee, K. M. Ok, *Eur. J. Inorg. Chem.* **2021**, 426–434.
[42] H.-Y. Liu, H.-Y. Zhang, X.-G. Chen, R.-G. Xiong, *J. Am. Chem. Soc.* **2020**, *142*, 15205–15218.
[43] M. Ma¸czka, A. Gagor, J. K. Zaréba, D. Stefanska, M. Drozd, S. Balciunas, M. Šimėnas, J. Banys, A. Sieradzki, *Chem. Mater.* **2020**, *32*, 4072–4082.
[44] C. Yuan, X. Li, S. Semin, Y. Feng, T. Rasing, J. Xu, *Nano Lett.* **2018**, *18*, 5411–5417.
[45] Y. Zeng, C.-L. Hu, W.-J. Xu, T.-W. Zeng, Z.-X. Zhu, X.-X. Chen, D.-X. Liu, Y.-J. Chen, Y.-B. Zhang, W.-X. Zhang, X.-M. Chen, *Angew. Chem. Int. Ed.* **2022**, *61*, e202110082; *Angew. Chem.* **2022**, *134*, e202110082.
[46] D. Chen, S. Hao, L. Fan, Y. Guo, J. Yao, C. Wolverton, M. G. Kanatzidis, J. Zhao, Q. Liu, *Chem. Mater.* **2021**, *33*, 8106–8111.
[47] K. M. Ok, *Chem. Commun.* **2019**, *55*, 12737–12748.
[48] C. C. Stoumpos, L. Frazer, D. J. Clark, Y. S. Kim, S. H. Rhim, A. J. Freeman, J. B. Ketterson, J. I. Jang, M. G. Kanatzidis, *J. Am. Chem. Soc.* **2015**, *137*, 6804–6819.
[49] P. S. Halasyamani, *Chem. Mater.* **2004**, *16*, 3586–3592.
[50] K. M. Ok, P. S. Halasyamani, D. Casanova, M. Llunell, P. Alemany, S. Alvarez, *Chem. Mater.* **2006**, *18*, 3176–3183.
[51] Y. Zhang, E. Parsonnet, A. Fernandez, M. Griffin Sinéad, H. Huyan, C.-K. Lin, T. Lei, J. Jin, S. Barnard Edward, A. Raja, P. Behera, X. Pan, R. Ramesh, P. Yang, *Sci. Adv.* **2022**, *8*, eabj5881.
[52] Z.-G. Lin, L.-C. Tang, C.-P. Chou, *Inorg. Chem.* **2008**, *47*, 2362–2367.
[53] G. Kieslich, S. Sun, A. K. Cheetham, *Chem. Sci.* **2015**, *6*, 3430–3433.
[54] J. Zhang, N. Su, C. Yang, J. Qin, N. Ye, B. Wu, C. Chen, *Proc. SPIE* **1998**, *3556*, 1.
[55] L. C. Tang, J. Y. Huang, C. S. Chang, M. H. Lee, L. Q. Liu, *J. Phys. Condens. Matter* **2005**, *17*, 7275–7286.
[56] Y. Dang, C. Zhong, G. Zhang, D. Ju, L. Wang, S. Xia, H. Xia, X. Tao, *Chem. Mater.* **2016**, *28*, 6968–6974.
[57] P.-P. Shi, Q. Ye, Q. Li, H.-T. Wang, D.-W. Fu, Y. Zhang, R.-G. Xiong, *Chem. Mater.* **2014**, *26*, 6042–6049.
[58] C. Ji, S. Wang, S. Liu, Z. Sun, J. Zhang, L. Li, J. Luo, *Chem. Mater.* **2017**, *29*, 3251–3256.
[59] S. Liu, Z. Sun, C. Ji, L. Li, S. Zhao, J. Luo, *Chem. Commun.* **2017**, *53*, 7669–7672.
[60] W.-J. Xu, C.-T. He, C.-M. Ji, S.-L. Chen, R.-K. Huang, R.-B. Lin, W. Xue, J.-H. Luo, W.-X. Zhang, X.-M. Chen, *Adv. Mater.* **2016**, *28*, 5886–5890.
[61] L.-S. Li, Y.-H. Tan, W.-J. Wei, H.-Q. Gao, Y.-Z. Tang, X.-B. Han, *ACS Appl. Mater. Interfaces* **2021**, *13*, 2044–2051.
[62] S. Liu, L. He, Y. Wang, P. Shi, Q. Ye, *Chin. Chem. Lett.* **2022**, *33*, 1032–1036.
[63] D. J. Clark, C. C. Stoumpos, F. O. Saouma, M. G. Kanatzidis, J. I. Jang, *Phys. Rev. B* **2016**, *93*, 195202.
[64] K. Wu, Y. Yang, L. Gao, *Coord. Chem. Rev.* **2020**, *418*, 213380.
[65] S. J. Clark, C. D. Flint, J. D. Donaldson, *J. Phys. Chem. Solids* **1981**, *42*, 133–135.
[66] C. Katan, L. Pedesseau, M. Kepenekian, A. Rolland, J. Even, *J. Mater. Chem. A* **2015**, *3*, 9232–9240.
[67] X. Lü, C. Stoumpos, Q. Hu, X. Ma, D. Zhang, S. Guo, J. Hoffman, K. Bu, X. Guo, Y. Wang, C. Ji, H. Chen, H. Xu, Q. Jia, W. Yang, M. G. Kanatzidis, H.-K. Mao, *Natl. Sci. Rev.* **2021**, *8*, nwaa288.
[68] J.-H. Cha, J. H. Han, W. Yin, C. Park, Y. Park, T. K. Ahn, J. H. Cho, D.-Y. Jung, *J. Phys. Chem. Lett.* **2017**, *8*, 565–570.
[69] D. B. Mitzi, *Chem. Mater.* **1996**, *8*, 791–800.
[70] P. Cheng, T. Wu, J. Zhang, Y. Li, J. Liu, L. Jiang, X. Mao, R.-F. Lu, W.-Q. Deng, K. Han, *J. Phys. Chem. Lett.* **2017**, *8*, 4402–4406.
[71] V. Morad, Y. Shynkarenko, S. Yakunin, A. Brumberg, R. D. Schaller, M. V. Kovalenko, *J. Am. Chem. Soc.* **2019**, *141*, 9764–9768.
[72] C. Wehrenfennig, M. Liu, H. J. Snaith, M. B. Johnston, L. M. Herz, *J. Phys. Chem. Lett.* **2014**, *5*, 1300–1306.
[73] I. Spanopoulos, I. Hadar, W. Ke, P. Guo, E. M. Mozur, E. Morgan, S. Wang, D. Zheng, S. Padgaonkar, G. N. Manjunatha Reddy, E. A. Weiss, M. C. Hersam, R. Seshadri, R. D. Schaller, M. G. Kanatzidis, *J. Am. Chem. Soc.* **2021**, *143*, 7069–7080.
[74] M. Ma¸czka, M. Ptak, A. Ga¸gor, D. Stefańska, J. K. Zaréba, A. Sieradzki, *Chem. Mater.* **2020**, *32*, 1667–1673.
[75] L.-y. Huang, W. R. L. Lambrecht, *Phys. Rev. B* **2016**, *94*, 115202.
[76] L.-C. Tang, Y.-C. Chang, J.-Y. Huang, M.-H. Lee, C.-S. Chang, *Jpn. J. Appl. Phys.* **2009**, *48*, 112402.
[77] S. K. Kurtz, T. T. Perry, *J. Appl. Phys.* **1968**, *39*, 3798–3813.
[78] R. C. Eckardt, H. Masuda, Y. X. Fan, R. L. Byer, *IEEE J. Quantum Electron.* **1990**, *26*, 922–933.
[79] W. Song, G.-Y. Guo, S. Huang, L. Yang, L. Yang, *Phys. Rev. Appl.* **2020**, *13*, 014052.
[80] G. Zou, C. Lin, H. Jo, G. Nam, T.-S. You, K. M. Ok, *Angew. Chem. Int. Ed.* **2016**, *55*, 12078–12082; *Angew. Chem.* **2016**, *128*, 12257–12261.
[81] E. J. Cho, S.-J. Oh, H. Jo, J. Lee, T.-S. You, K. M. Ok, *Inorg. Chem.* **2019**, *58*, 2183–2190.
[82] C.-L. Hu, J.-G. Mao, *J. Phys. Condens. Matter* **2010**, *22*, 155801.
[83] X.-S. Xing, R.-J. Sa, P.-X. Li, N.-N. Zhang, Z.-Y. Zhou, B.-W. Liu, J. Liu, M.-S. Wang, G.-C. Guo, *Chem. Sci.* **2017**, *8*, 7751–7757.
[84] H. Tan, F. Che, M. Wei, Y. Zhao, M. I. Saidaminov, P. Todorović, D. Broberg, G. Walters, F. Tan, T. Zhuang, B. Sun, Z. Liang, H. Yuan, E. Fron, J. Kim, Z. Yang, O. Voznyy, M. Asta, E. H. Sargent, *Nat. Commun.* **2018**, *9*, 3100.
[85] J. M. Frost, K. T. Butler, F. Brivio, C. H. Hendon, M. van Schilfgaarde, A. Walsh, *Nano Lett.* **2014**, *14*, 2584–2590.
[86] Deposition numbers 2179599, 2179600, 2179601, 2179602, 2179603, 2179604, and 2179605 contain the supplementary crystallographic data for this paper. These data are provided free of charge by the joint Cambridge Crystallographic Data Centre and Fachinformationszentrum Karlsruhe Access Structures service.

Manuscript received: June 17, 2022
Accepted manuscript online: August 31, 2022
Version of record online: ■■, ■■

Research Articles

Perovskites

Y. Liu, Y.-P. Gong, S. Geng, M.-L. Feng, D. Manidaki, Z. Deng, C. C. Stoumpos, P. Canepa,* Z. Xiao, W.-X. Zhang, L. Mao* **e202208875**

Hybrid Germanium Bromide Perovskites with Tunable Second Harmonic Generation

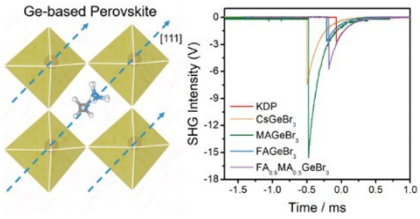

A new family of non-centrosymmetric hybrid Ge-based bromide perovskites are reported, showing second harmonic generation (SHG) responses. The largest SHG signal from $CH_3NH_3GeBr_3$ is likely due to the perferable alignment of the polar cation with the lone pair electrons of Ge^{2+} along the [111] direction.